

Modulation of Bessel-like vector vortex beam using the resonant magneto-optical effect in rubidium vapor

Yan Ma(马燕), Xin Yang(杨欣), Hong Chang(常虹), Ming-Tao Cao(曹明涛), Xiao-Fei Zhang(张晓斐), Rui-Fang Dong(董瑞芳), and Shou-Gang Zhang(张首刚)

Citation : Chin. Phys. B, 2025, 34 (**2**): 024202. DOI: 10.1088/1674-1056/ad9c43
Journal homepage: http://cpb.iphy.ac.cn; http://iopscience.iop.org/cpb

What follows is a list of articles you may be interested in

Superradiance of ultracold cesium Rydberg $|65D_{5/2}> \rightarrow |66P_{3/2}>$

Liping Hao(郝丽萍), Xiaoxuan Han(韩小萱), Suying Bai(白素英), Xiufen You(游秀芬), Yuechun Jiao(焦月春), and Jianming Zhao(赵建明)
Chin. Phys. B, 2024, 33 (**5**): 054204. DOI: 10.1088/1674-1056/ad20da

Generation of structure light in probe absorption spectrum via microwave-driven Y-type atomic system

Muhammad Saeed and Muqaddar Abbas
Chin. Phys. B, 2023, 32 (**12**): 124211. DOI: 10.1088/1674-1056/aceee7

Ground-state phase diagram, symmetries, excitation spectra and finite-frequency scaling of the two-mode quantum Rabi model

Yue Chen(陈越), Maoxin Liu(刘卯鑫), and Xiaosong Chen(陈晓松)
Chin. Phys. B, 2023, 32 (**10**): 104213. DOI: 10.1088/1674-1056/acea66

Tunable magnomechanically induced transparency and fast-slow light in a hybrid cavity magnomechanical system

Qinghong Liao(廖庆洪), Kun Peng(彭坤), and Haiyan Qiu(邱海燕)
Chin. Phys. B, 2023, 32 (**5**): 054205. DOI: 10.1088/1674-1056/acaf2b

Nonreciprocal two-photon transmission and statistics in a chiral waveguide QED system

Lei Wang(王磊), Zhen Yi(伊珍), Li-Hui Sun(孙利辉), and Wen-Ju Gu(谷文举)
Chin. Phys. B, 2022, 31 (**5**): 054206. DOI: 10.1088/1674-1056/ac3ecc

---

Modulation of Bessel-like vector vortex beam using the resonant magneto-optical effect in rubidium vapor

Yan Ma(马燕)[1,2], Xin Yang(杨欣)[3], Hong Chang(常虹)[1,2], Ming-Tao Cao(曹明涛)[1,2,†], Xiao-Fei Zhang(张晓斐)[4], Rui-Fang Dong(董瑞芳)[1,2,5,‡], and Shou-Gang Zhang(张首刚)[1,2]

[1] *Key Laboratory of Time Reference and Applications, National Time Service Center, Chinese Academy of Sciences (CAS), Xi'an* 710600, *China*
[2] *School of Astronomy and Space Science, University of Chinese Academy of Sciences, Beijing* 100049, *China*
[3] *Ministry of Education Key Laboratory for Nonequilibrium Synthesis and Modulation of Condensed Matter, Shaanxi Province Key Laboratory of Quantum Information and Quantum Optoelectronic Devices, School of Physics, Xi'an Jiaotong University, Xi'an* 710049, *China*
[4] *Department of Physics, Shaanxi University of Science and Technology, Xi'an* 710021, *China*
[5] *Hefei National Laboratory, Hefei* 230088, *China*

(Received 20 October 2024; revised manuscript received 25 November 2024; accepted manuscript online 10 December 2024)

The Bessel-like vector vortex beam (BlVVB) has gained increasing significance across numerous applications. However, its practical application is restricted by manufacturing difficulties and polarization manipulation. Thus, the ability to manipulate its degrees of freedom is highly desirable. In this paper, the full-domain polarization modulation of BlVVB within a hot atomic ensemble has been investigated. We begin with the theoretical analysis of the resonant magneto-optical effect of atoms with a horizontal linear-polarized beam and experimentally demonstrate precise manipulation of the polarization state across the entire domain of the BlVVB, achieving an error margin of less than 3° at various cross-sectional points. Our study provides a novel approach for the modulation of BlVVB based on atomic media, which holds potential applications in sensitive vector magnetometers, optical communications, and signal processing.

Keywords: Bessel-like vector vortex beam, resonant magneto-optical effect, polarization modulation, Rb atomic ensemble

PACS: 42.50.Ct, 78.20.Ls, 42.60.Jf, 42.81.Gs

DOI: 10.1088/1674-1056/ad9c43 **CSTR:** 32038.14.CPB.ad9c43

1. Introduction

The optical properties of Bessel-like vector vortex beam (BlVVB) with spatially inhomogeneous polarization states have attracted significant attention due to its potential applications in fields such as particle orientation analysis[1,2] and atomic magnetometry.[3–5] Theoretically, BlVVB can be represented as a vector superposition of two orthogonally polarized Gaussian modes,[6] exhibiting a Bessel-type phase distribution but with a Gaussian-type profile,[7] and demonstrating unique radial periodicity and angular uniformity in its polarization properties. The transverse polarization state of BlVVB can be used to increase the information transmission capacity for both classical and quantum optical communications primarily, which is critical for free-space optical communication and other practical applications.[8,9] However, the BlVVB faces significant challenges in beam manipulation. Since the polarization and transverse phase distribution of BlVVB can only be modulated homogeneously by wave plates in linear optical systems. Thus, the development of a controllable polarization manipulation scheme for BlVVB is highly desirable.

The atom–light interactions provide an excellent platform for polarization manipulation. Budker[10] elaborated on the resonant magneto-optical effect in atomic media as early as 2008. Since then, researchers have used this effect to study the polarization rotation of scalar beams[11,12] and used it for magnetic field detection.[3,13] With the rapid development of space-variable polarization beams,[14,15] the polarization rotation control of vector beams using resonant magneto-optics has been reported and used for polarization shaping.[16–18] Based on the thermal atomic vapors, Shi *et al.*[19] studied the rotation of light with orbital angular momentum; Zhang *et al.*[20] achieved real-time rapid shaping of vector beams. It has been widespread to modulate the polarization freedom of light fields using the magneto-optical effect in atomic media. However, most of the above works have focused on observations of its projected horizontally polarized component, and the assessment of the polarization rotation angle is more coarse. The quantitative analysis of the full-domain polarization state of the vector beam has not been reported.

In this paper, we experimentally demonstrate precise manipulation of the polarization state across the entire domain of the BlVVB, achieving an error margin of less than 3° at various cross-sectional points. By leveraging the high Verdet

†Corresponding author. E-mail: mingtaocao@ntsc.ac.cn
‡Corresponding author. E-mail: dongruifang@ntsc.ac.cn

© 2025 Chinese Physical Society and IOP Publishing Ltd. All rights, including for text and data mining, AI training, and similar technologies, are reserved.

constant[21] of rubidium, we obtained a controllable and stable circular birefringent system associated with the magnetic field intensity. Combining a rubidium vapor cell with BlVVB allows for full-domain polarization modulation. In addition, we have analyzed the evolution of the modulated BlVVB after the atomic cell in free space, which behaves similarly to the original beam. Our scheme provides a novel way to modulate BlVVB. It paves the way for tailored "pixel-level" polarization control, which may have a robust foundation for spatial magnetic field measurements, sensitive vector magnetometers, and optical communications.

This paper is organized in the following sections. Section 2 describes the BlVVB and the theoretical formalism for the polarization rotation angle induced by the resonant magneto-optical effect. Section 3 gives the details of the experimental setup. Section 4 collates all the experimental results and discussions. Finally, Section 5 presents our conclusions.

2. Concept and theoretical considerations

The Bessel-like vector vortex beam can be described as the superposition of two orthogonal modes. This beam features a Bessel-type radial phase distribution but a Gaussian-type profile. In the standard cartesian basis, the initial state in this work is expressed as

$$E = E_x \cdot \cos\left(\frac{\rho}{2\pi \cdot n} + \varphi_0\right) e_x + E_y \cdot \sin\left(\frac{\rho}{2\pi \cdot n} + \varphi_0\right) e_y, \quad (1)$$

where E_x and E_y are the horizontal and vertical electric field components, respectively. These components are defined as

$$E_x = \cos(\alpha) \exp\left(-\rho^2/\omega^2\right),$$

$$E_y = \sin(\alpha)\, \mathrm{e}^{\mathrm{i}\theta} \exp\left(-\rho^2/\omega^2\right), \quad (2)$$

where parameters α and θ represent the relative amplitude and the phase between the two modes, respectively. The parameter φ_0 is the initial phase. The ρ is the radial distance from the beam axis. The ω is the beam waist radius, and n is the phase period factor.

According to this expression, the theoretical intensity patterns and polarization distribution of the BlVVB are plotted in Fig. 1(a). To visualize the cross-sectional polarization distribution, the beam profile is initially divided into 5 equal rings from the center to the edge, with the polarization state calculated at 10° intervals for each ring. This approach ensures a clear representation of the polarization states. For a more detailed analysis, the number of rings in the MATLAB program was set to 30. In Fig. 1(a), the azimuth angles along the radial direction at 0-radian, referred to as the "radial azimuth angles", are extracted and plotted in Fig. 1(b). Similarly, the azimuth angles along the angular direction of the first 6 rings, marked by blue arrows, are referred to as "angular azimuth angles" and are plotted in Fig. 1(c). It can be observed that the polarization distribution exhibits radial periodicity and angular uniformity. Notably, the radial azimuth angles along any arbitrary radius show similar characteristics to those along the 0-radian direction, as the azimuth angles remain consistent along the rings. This regularity in the polarization distribution provides a solid foundation for the subsequent quantitative analysis in later experiments.

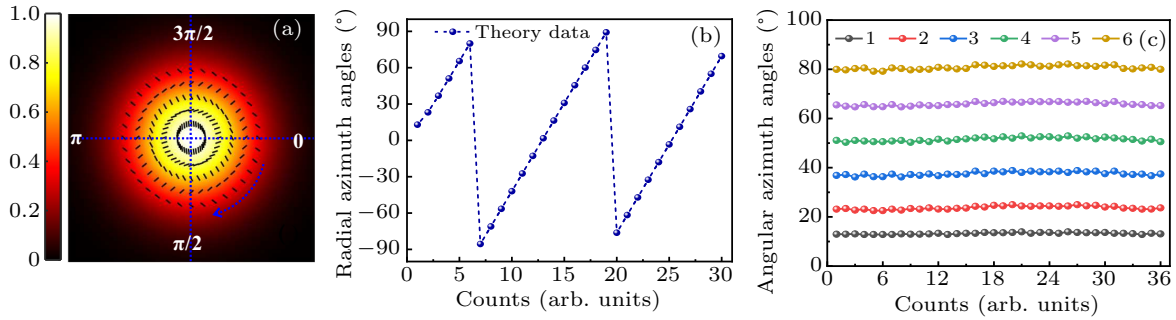


Fig. 1. (a) The theoretical intensity pattern and polarization distribution of the BlVVB. (b) Along the radial direction, the polarization distribution shows periodicity. (c) Along the angular direction, the polarization distribution shows uniformity ($\varphi_0 = 0$, $\alpha = \pi/4$, $\theta = 0$).

To provide a clearer picture of the light–atom interaction between the BlVVB and the atoms, we start with the theoretical analysis of the polarization modulation mechanism. In agreement with the experimental resonance frequencies, the simplified four-level system includes the ground states. $5^2S_{1/2}$, $F_g = 2$, $m = \pm 1, 0$ and the excited states $5^2P_{3/2}$ $F_e = 1$, $m = 0$ of the ^{87}Rb D_1 line, is considered, as illustrated in Fig. 2(a).

In addition, linearly polarized light incident on an atomic sample can be decomposed into right- (σ_+) and left- (σ_-) circularly polarized components. Since the arbitrary polarization states of the transverse cross-section of BlVVB are located on the Poincaré equator, each point corresponds to a linearly polarized state. Thus, the full-domain polarization modulation of BlVVB can be understood through the resonant magneto-optical effect of linearly polarized light interacting with an atomic medium.

In the absence of the magnetic field, the Zeeman sublevels

are degenerate. When a longitudinal magnetic field B_z is applied to the atomic sample along the direction of light propagation, the Zeeman shifts between adjacent magnetic sublevels ($g_F\mu_B B_z$, where g_F is the Landé factor, and μ_B is the Bohr magneton) lead to different resonance frequencies for the two circular polarizations, resulting in a difference in the refractive indices of the σ_+ and σ_- components. The refractive index difference can be expressed as[22,23]

$$\Delta n = -2\pi\chi_0 \frac{4g_F\mu_B B_z/\gamma_0}{(2g_F\mu_B B_z/\gamma_0)^2 + [1 - 2i(\omega - \omega_0/\gamma_0)]^2}, \quad (3)$$

which signifies a difference in phase velocities of the two circular components. Where χ_0 is the amplitude of the linear susceptibility. γ_0 is the spontaneous decay rate of the excited state. ω is the light frequency, and ω_0 is the atomic resonance frequency.

The difference in the real parts of the indices of refraction causes optical rotation. A relative phase shift is acquired as the light propagates through the atomic vapor. Therefore, the plane of polarization rotates by an angle

$$\varphi = \frac{2\pi\chi_0\omega\ell}{c} \cdot \frac{a\left[1 + a^2 - (2\Delta/\gamma_0)^2\right]}{(2\Delta/\gamma_0)^2 + \left[1 + a^2 - (2\Delta/\gamma_0)^2\right]^2}, \quad (4)$$

where $a = 2g_F\mu_B B_z/\gamma_0$. According to the above equation, the magneto-optical rotation angle dependence on the magnetic field is plotted when the light frequency resonates with the atomic frequency, as shown in Fig. 2(b). It should be emphasized that magneto-optical rotation arises due to a relative shift in the refractive indices for right- and left-circularly polarized components. As a result, the rotation angle integrated over the magnetic field is zero and exhibits a dispersion-like curve. That is positive and negative magnetic fields of the same magnitude cause equal polarization rotation angles.

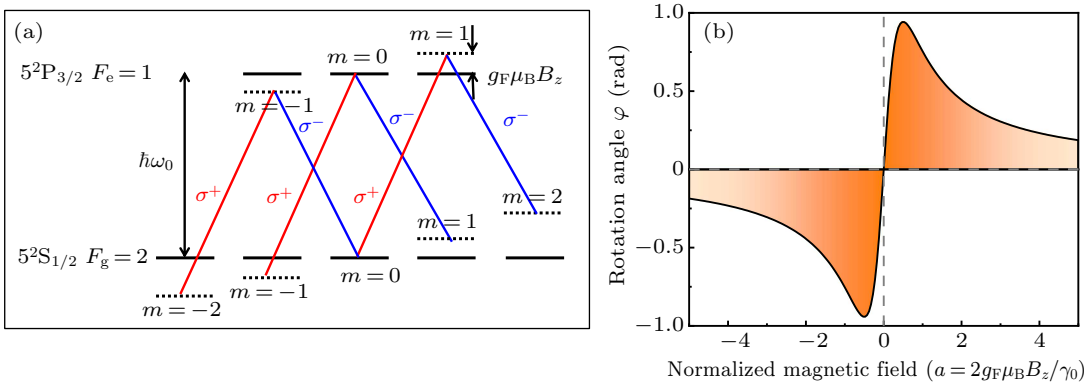


Fig. 2. (a) Schematic diagram of energy levels transition from $F_g = 2$ to $F_e = 1$ of the ^{87}Rb D_1 line with a magnetic field. σ^+: right-hand polarization beam; σ^-: left-hand polarization beam. (b) The dependence of the polarization rotation angle as a function of longitudinal magnetic field for the case of zero detuning theoretically ($\omega = \omega_0$).

3. Experimental setup

Figure 3(a) illustrates the experiment setup. The 795-nm laser beam from an external cavity diode laser (ECDL) is divided into two parts. One part is sent to a saturated absorption spectroscopy (SAS) installation for the frequency locking. The frequency resonates to $5^2S_{1/2}$, $F_g = 2 \rightarrow 5^2P_{3/2}$, $F_e = 1$ transition of ^{87}Rb D_1 line. Another part is coupled into a single-mode fiber (SMF) to obtain a perfect Gaussian mode. The following half-wave plate (HWP) and a polarization beam splitter (PBS) are used to change the beam power, and the beam's power is 3 mW. Then, another HWP is applied to adjust the linear polarization state of the incident beam.

In order to generate the BlVVB, we use a special polarizer with optical axes periodically varying along the radial direction namely a radial varying polarizer (RVP), which introduces the Pancharatnam–Berry (PB) geometrical phase in the incident light. Subsequently, the generated vector beam passes through a 5-cm-long atomic vapor cell containing the ^{87}Rb atom. The atomic cell is enclosed inside a three-layer μ metal magnetic shield to prevent external stray magnetic fields, and the measured residual magnetic field is less than 2 mGs (1 Gs = 10^{-4} T) in the longitudinal direction. A solenoid coil is placed inside the inner layer of the magnetic shield, which provides a homogeneous longitudinal magnetic field along the direction of the light propagation. In the experiment, the longitudinal magnetic field could be controlled by adjusting the coil's current, and the vapor cell's temperature was set to 77 °C.

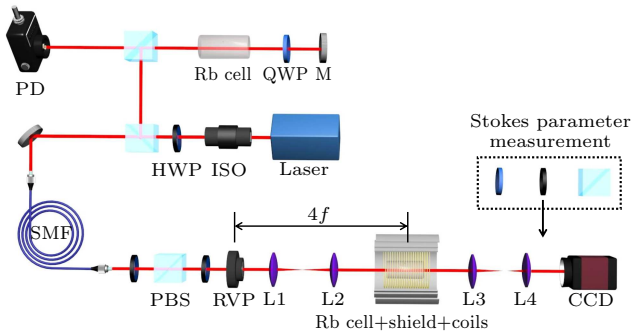


Fig. 3. (a) Experimental setup. ISO: optical isolator; SMF: single-mode fiber; M: mirror; PD: photodetector; PBS: polarization beam splitter; HWP: half-wave plate; QWP: quarter-wave plate; RVP: radial varying polarizer; CCD: charge-coupled device camera; L1–L4: plano-convex lenses.

Since the BlVVB evolves severely in free space, the polarization states vary rapidly in the propagation. In order to observe the interaction between the BlVVB and atoms, we imaging the BlVVB into the atom cell using a $4f$ telescope with a focal length of 250 mm. The charge-coupled device (CCD) camera is placed after another $4f$ imaging telescope to capture the BlVVB images modulated by rubidium atoms.

4. Experimental results and discussion

Firstly, we analyze the polarization state of the generated BlVVB. To quantify the transverse polarization states more precisely, we measure the horizontal, vertical, diagonal, anti-diagonal, left and right circular polarization components of the BlVVB by combining wave plates and PBS.[24,25] The Stokes parameter ($S=[S_0,S_1,S_2,S_3]$) can be subsequently calculated using the following equations:

$$\begin{aligned} S_0 &= I_{\mathrm{H}}+I_{\mathrm{V}} = I(0^\circ,0^\circ)+I(90^\circ,45^\circ),\\ S_1 &= I_{\mathrm{H}}-I_{\mathrm{V}} = I(0^\circ,0^\circ)-I(90^\circ,45^\circ),\\ S_2 &= I_{\mathrm{A}}-I_{\mathrm{D}} = I(45^\circ,22.5^\circ)-I(135^\circ,67.5^\circ),\\ S_3 &= I_{\mathrm{R}}-I_{\mathrm{L}} = I(135^\circ,0^\circ)-I(45^\circ,0^\circ), \end{aligned} \tag{5}$$

where $I(\alpha,\beta)$ represents the intensity when the optical axes of QWP and HWP rotated by the angle α, β with respect to the fast axis, respectively. Thereby, the normalized Stokes parameters $S_i=S_i/S_0$ $(i=0,1,2,3)$ can be acquired, as shown in the first row of Fig. 4. The far left depicts the polarization distribution of BlVVB.

Then, we turn to the polarization modulation of BlVVB with atoms. In our scheme, the laser is locked to $5^2\mathrm{S}_{1/2}$, $F_{\mathrm{g}}=2\rightarrow 5^2\mathrm{P}_{3/2}$, $F_{\mathrm{e}}=1$ transition of ^{87}Rb D_1 line, and the schematic energy transition diagram is depicted in Fig. 2(a). When an axial magnetic field is applied, the Zeeman effect induces the splitting of the hyperfine energy levels. In the experiment, we define the quantization axis as the propagation direction along the beam. Therefore, linear polarization can be considered as a superposition of the left and right circular polarization components. The beam with σ^+ polarization couples the Zeeman sublevel, satisfying the transition rule $\Delta m_{\mathrm{F}}=+1$, and σ^- polarization couples the transition satisfying $\Delta m_{\mathrm{F}}=-1$.

The polarization state starts to rotate homogeneously when the magnetic field increases along the quantization axis. We can observe the polarization rotation across the entire domain of the BlVVB. The polarization states of BlVVB after rotation are also reconstructed by calculating the Stokes parameters. The results are shown in the second row of Fig. 4. In order to view the uniformity of the polarization along the azimuth, we pick up 5 rings equally from the beam center to the edge and calculate the polarization azimuth angle along the radius at intervals of 10°. It is worth mentioning that we averaged the grayscale value over a grid of 5×5 square pixels on the CCD camera to obtain more convincing data.

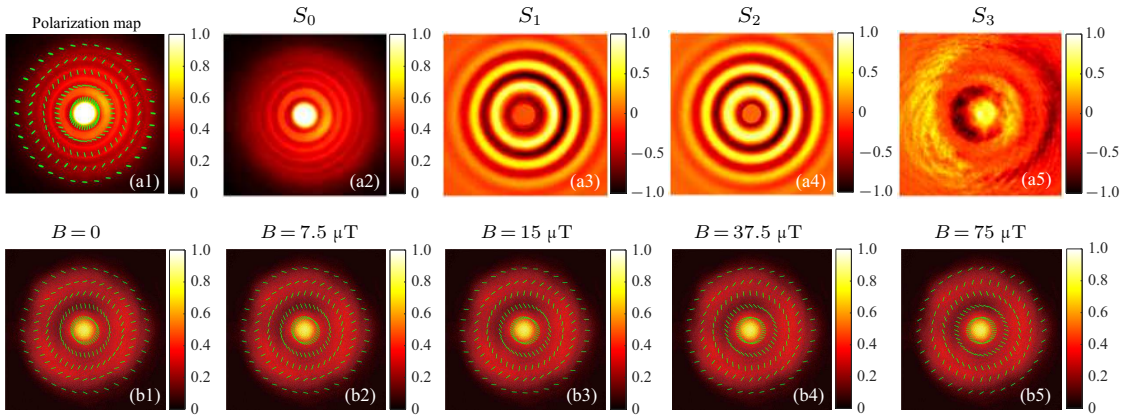


Fig. 4. (a1)–(a5) First row: the polarization distribution and the normalized Stokes parameter $S=[S_0,S_1,S_2,S_3]$ of the initial generated BlVVB. Panels (b1)–(b5) are the polarization distributions of the BlVVB after passing through the atom vaper cell with increasing positive magnetic fields.

As analyzed in the theoretical part, the BlVVB profile was divided into 30 rings to analyze the polarization distribution characteristics more quantitatively. Radial azimuth angles at 0 radian after rotation were extracted (as shown in the indicated direction in Fig. 1(a)). Radial azimuth angles under various magnetic fields are depicted in Fig. 5(a), corresponding to Figs. 4(b1)–4(b5) at 0 radian, respectively. It can be observed that the azimuthal angle is periodic along the radial direction without a magnetic field. With increasing positive magnetic field strength, the angle rotates while maintaining periodicity. Therefore, the radial periodic polarization characteristics remain unchanged before and after polarization rotation modulation. Furthermore, it should be noted that the radial azimuth angles at $\pi/2$, π, and $3\pi/2$ are similar to those at 0 radian; therefore, only the 0 radian direction comparison is presented here.

Subsequently, to compare the degree of deflection of the polarization orientation under different magnetic fields, we calculated the rotation angle of the polarization-modulated

BlVVB at 0 radian. That is to say, the azimuthal angle at 0 radian after polarization modulation subtracted those from the zero magnetic field, respectively. The results of the polarization rotation angles are presented in Fig. 5(b). The purple, yellow, green, and blue makers indicate the rotation angles along the radial direction for magnetic field strengths of 7.5 μT, 15 μT, 37.5 μT, and 75 μT, respectively. The dashed lines of the same colors represent the average of the scatter data. It was found that the rotation angles along the radial direction were nearly uniformly aligned around a specific value. Corresponding to different magnetic field strengths, the rotation angles are 9.80°, 19.73°, 35.49°, and 55.43°, respectively.

Following this, the radial polarization rotation angles (with respect to the zero magnetic field) were statistically analyzed along the complete circumference within 2π at 10° intervals. The standard deviation of the mean is shown in Fig. 5(c). The errors at all points remained within 3°. As a result, this magnetic field-induced stable circular birefringence atomic system allows precise modulation of the full-domain polarization of the BlVVB. A new BlVVB was generated after each point polarization was rotated by a specific angle while maintaining the initial radial periodicity and angular uniformity of the polarization characteristics.

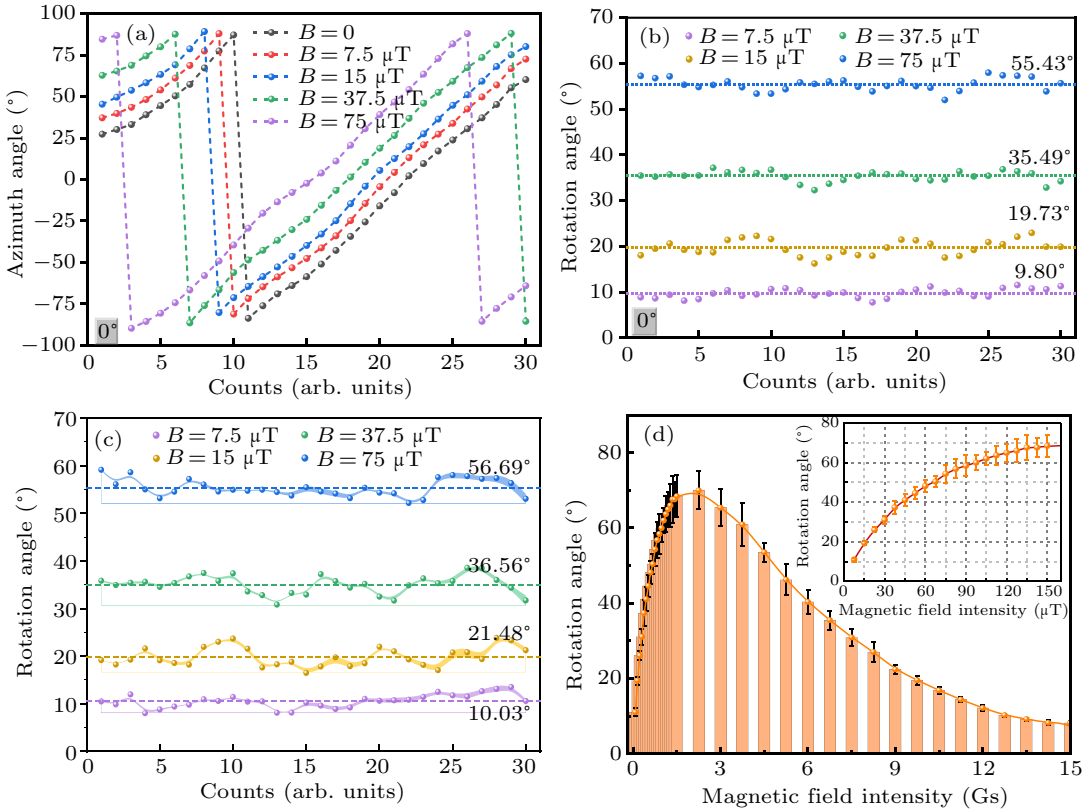


Fig. 5. Radial azimuthal angles under different magnetic fields: (a) radial polarization azimuthal angle along the 0 radian direction; (b) radial polarization rotation angle relative to the zero magnetic field, with the dashed line representing the average of the scatter data; (c) statistical analysis of the radial polarization rotation angle at 10° intervals over a 2π range. (d) The dependence of the rotation angle of the horizontally polarized Gaussian beam on the positive magnetic field. The inset in the top right corner shows an enlarged view of the weak magnetic field (0 μT–150 μT).

Then, to ensure the stability and accuracy of the polarization modulation of BlVVB by the atomic medium under different magnetic fields, we removed the RVP from the experimental setup and replaced the Stokes parameter measurement device with a polarization analyzer, and other experiment conditions were kept the same as previously. In this case, a horizontal linear polarized Gaussian beam passes through the atomic medium. The relationship between the polarization rotation angle and the magnetic field intensity is shown in Fig. 5(d), where the insert in the upper right corner is an enlarged view in the case of a weak magnetic field. It can be seen that for the same magnetic field, the BlVVB full-domain polarization rotation angle in Fig. 5(c) is highly consistent with the rotation angles of the horizontally polarized beam in the enlarged view of Fig. 5(d). For example, at $B = 37.5$ μT, the polarization rotation at all points of the BlVVB cross-section is 36.56°, and the horizontally polarized Gaussian beam is rotated by $37.36° \pm 2.85°$. It is shown that the BlVVB full-domain polarization can be modulated on demand using the scalar Gaussian beam magneto-optical rotation angle as a reference. Of course, this stable atomic system can also be used to modulate the polarization degree of freedom of other vector beams, with the advantage of fast response and high accuracy. Here, we performed three parallel measurements to minimize accidental errors. It is evident that the rotation angle initially experiences a quick increase, followed by a gradual decrease

as the positive magnetic field goes up. The maximum rotation angle of 70° is reached at $B = 150$ μT. It is essential to mention that by changing the direction of the magnetic field, the rotation of polarization changes from counterclockwise to clockwise. If the magnetic field is uniformly distributed in the cell scale, the resulting curve exhibits symmetry about the zero magnetic field, consistent with the theoretical calculations in Fig. 2(b).

In addition, we analyzed the evolution of the modulated BlVVB after the atomic cell in free space, which behaves similarly to the original beam. The propagation of the BlVVB is shown in Figs. 6(a1) and 6(a2). Panel (a1) presents the transverse intensity profile of the horizontal component of the BlVVB at different distances from the RVP. At the same time, panel (a2) displays the normalized intensity curve at 0 radian at distances of 25 cm, 50 cm, and 60 cm, respectively. As can be seen, the Rayleigh transmission distance of the BlVVB is very short, approximately 25 cm, and its radial periodic polarization distribution gradually disappears with increasing distance. Next, we observed the propagation of the modulated BlVVB. The propagation of the BlVVB with full-domain polarization rotated by 36.56°, i.e., the atomic cell in a 37.5-μT magnetic field, is shown in Figs. 6(b1)–6(b2). Here, panel (b1) shows the transverse intensity profile of the horizontal component of the BlVVB at different distances from the second 4f lens after atomic modulation, and panel (b2) presents the normalized intensity curve at distances of 25 cm, 50 cm, and 60 cm, respectively. It is observed that the modulated BlVVB undergoes significant evolution during propagation, with inevitable beam size expansion. Thus, the propagation characteristics of the BlVVB are maintained after full-domain polarization modulation. This method of modulating the polarization degree of freedom through the resonant magneto-optical effect of the atomic medium is feasible and can also be applied to other structured beams. It holds the potential to inspire new approaches to space magnetic field measurements.

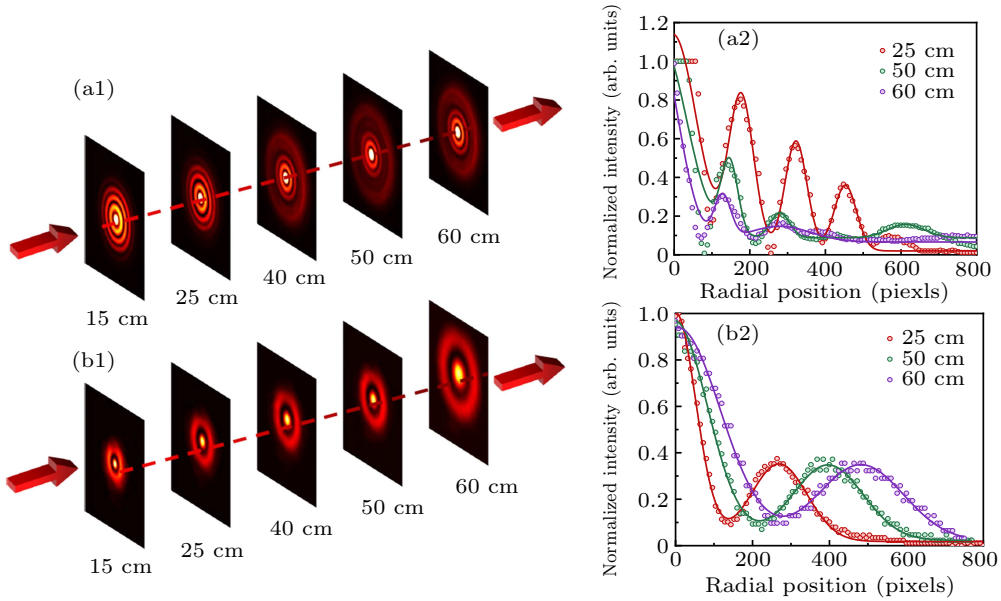


Fig. 6. Propagation evolution characteristics of BlVVB before and after being modulated. Panels (a1) and (b1) show the propagation characteristics of BlVVB after the RVP and the second 4F lens, respectively. Panels (a2) and (b2) represent the normalized intensity curve at 0 radian at 25 cm, 50 cm, and 60 cm, respectively.

5. Conclusions

In conclusion, this study successfully demonstrated full-domain polarization modulation of the Bessel-like vector vortex beam (BlVVB) within thermal atomic ensembles. By leveraging the high Verdet constant of rubidium vapor, we established a controllable and stable circular birefringent system. The resonant magneto-optical effect allowed precise manipulation of the BlVVB's polarization states, with errors at various points of the cross-section not exceeding 3°. The propagation characteristics of the modulated beam closely resemble those of the original beam, The feasibility and effectiveness of polarization modulation may also apply to other structured beams. This approach holds potential applications in sensitive magnetometers, optical communications, and signal processing. Future work may explore broader applications and innovations utilizing this stable atomic media system.

Acknowledgements

Project supported by the National Natural Science Foundation of China (Grant Nos. 12033007, 61801458, 12103058, 12203058, 12074309, and 61875205), the Key Project of Frontier Science Research of the Chinese Academy of Sciences (Grant No. QYZDB-SSW-SLH007), the Strategic Priority Research Program of CAS (Grant No. XDC07020200), the Youth Innovation Promotion Association, CAS (Grant Nos. 2021408, 2022413, and 2023425), and the Research

on Highly Sensitive Long-Wave Receiver Based on Rydberg Atoms (Grant No. 1P2024000059).

References

[1] Li Z, Zhang N, Guo J, Guo Q, Yu T, Zhang M, Wang G, Gao X and Zhang X 2023 *Opt. Express* **31** 9299

[2] Dolan P R, Li X, Storteboom J and Gu M 2014 *Opt. Express* **22** 4379

[3] Reuschel P, Agio M and Flatae A M 2022 *Advanced Quantum Technologies* **5** 2200077

[4] Qiu S, Wang J, Castellucci F, Cao M, Zhang S, Clark T W, Franke-Arnold S, Gao H and Li F 2021 *Photon. Res.* **9** 2325

[5] Castellucci F, Clark T W, Selyem A, Wang J and Franke-Arnold S 2021 *Phys. Rev. Lett.* **127** 233202

[6] Liu Z, Liu Y, Ke Y, Liu Y, Shu W, Luo H and Wen S 2017 *Photon. Res.* **5** 15

[7] Zeng X, Li Z, Yang X, Xu J, Wang J, Wang C, Quan Q, Chen H, Wei D, Gao H and Li F 2024 *New J. Phys.* **26** 063029

[8] Zhao R Z, Huang L L, Tang C C, Li J J, Li X W, Wang Y T and Zentgraf T 2018 *Adv. Opt. Mater.* **6** 1800490

[9] Bao Y J, Ni J C and Qiu C W 2020 *Adv. Mater.* **32** 1905659

[10] Budker D, Gawlik W, Kimball D, Rochester S, Yashchuk V and Weis A 2002 *Rev. Mod. Phys.* **74** 1153

[11] Pandey K, Wasan A and Natarajan V 2008 *J. Phys. B: At. Mol. Opt. Phys.* **41** 225503

[12] Qiu S, Guo W, Cao M, Liu T, Han L, Liu H, Zhang P, Zhang S, Gao H and Li F 2012 *Chin. Opt. Lett.* **10** 052701

[13] Makarov A O, Brazhnikov D V and Goncharov A N 2023 *JETP Lett.* **117** 509

[14] Stern L, Szapiro A, Talker E and Levy U 2016 *Opt. Express* **24** 4834

[15] Szapiro A, Stern L and Levy U 2015 *Conference on Lasers and Electro-Optics (CLEO)*, pp. 1–2

[16] Daloi N and Dey T N 2022 *Opt. Express* **30** 21894

[17] Ghaderi Goran Abad M and Mahmoudi M 2021 *Sci. Rep.* **11** 5972

[18] Gibson C J, Bevington P, Oppo G L and Yao A M 2018 *Phys. Rev. A* **97** 033832

[19] Shi S, Ding D S, Zhou Z Y, Li Y, Zhang W and Shi B S 2015 *Appl. Phys. Lett.* **106** 261110

[20] Zhang L, Yang Y, Yang X, Gao H and Li F 2020 *J. Phys. B: At. Mol. Opt. Phys.* **53** 155404

[21] Srinivasan R 2007 *Current Science* **92** 298

[22] Auzinsh M, Budker D and Rochester S 2010 *Optically polarized atoms: understanding light-atom interactions* (Oxford: Oxford University Press) pp. 55–60

[23] Budker D, Kimball D F and DeMille D P 2004 *Atomic physics: an exploration through problems and solutions* (Oxford: Oxford University Press, USA) pp. 187–191

[24] Schaefer B, Collett E, Smyth R, Barrett D and Fraher B 2007 *American Journal of Physics* **75** 163

[25] Milione G, Sztul H I, Nolan D A and Alfano R R 2011 *Phys. Rev. Lett.* **107** 053601